ISSN: 2688-8645

Set-Membership Localization and Robust Detection-Point Selection for Interference Sources under Bounded Bearing Errors

Suqin Zhang *, Yanghao Luo, Shirong Su and Zhen Liu

School of Health and Medical Technology, Chengdu Neusoft University, Chengdu, Sichuan, China

* Corresponding author: Suqin Zhang

Abstract

Radio interference degrades spectrum access, and locating the emitter is the geometric core of its removal. This paper treats the bearing error as a known bound and develops a set-membership framework for the first two stages of that task: describing the set of admissible source positions from several bearings, measuring its size by the worst-case localisation diameter, and choosing the next detection point before the source position is known. Each bearing is represented by an angular domain of half-width ε, and the localisation region is the intersection of those domains with the circular target region. That intersection is unbounded exactly when the bearing intervals share a common direction, which for two observations reduces to the analytic test $\Delta\theta \le 2\varepsilon$; this replaces the finite bounding box that misclassifies near-degenerate configurations. Closed-form vertices and a rotating-calipers diameter give the region and its diameter in linear time, and the smallest disk containing the region is obtained exactly. The disk spanning the diameter does not always cover the region; Jung's theorem bounds the ratio by $2/\sqrt{3} = 1.1547$, and the bound is attained by an equilateral configuration. The second detection point is chosen by minimax optimisation over both the unknown source position and the unknown sign of the second bearing error, subject to worst-case reception feasibility. The recommended point is S2* = (−399.66, 1484.27) m; it lies on the reception boundary and gives a worst-case diameter of 131.36 m. The candidate region is an annular sector of half-width 40.2° whose 5 % accuracy band extends from 987 to 1016 m in radius. A Monte-Carlo study on 3000 admissible sources gives a mean diameter of 56.3 m at this point, against 95.0 m for a naive perpendicular placement.

Keywords

Set-membership Localization; Bearing-only Triangulation; Minimax Robustness; Minimum Enclosing Circle; Detection-point Selection.

1. Introduction

Radio-frequency interference is a first-order constraint on the use of the radio spectrum, and removing it requires finding the emitter. Operational practice divides the search into initial monitoring, regional screening and precise localisation. The first two stages delimit the area that contains the emitter with fixed stations, vehicles or unmanned aircraft; the final stage is carried out inside that area with a hand-held direction finder, and its duration dominates the cost of the operation. This paper addresses the geometric core of that stage: how to turn a set of bearings taken at known positions into a rigorous description of where the source can be, and how to choose the next measurement so that this description improves as much as possible.

A direction finder returns the azimuth of the maximum received field strength but no range, so localisation rests on triangulation. Two schools exist for handling the measurement error. The statistical school models the error as a random variable, linearises the observation equations

ISSN: 2688-8645

and reports a point estimate with a covariance or a dilution-of-precision figure [1, 2, 3, 4], and the optimal sensor-target geometries and observability metrics for that criterion are well understood [5, 6]. The set-membership school treats the error as a known bound and propagates the set of states compatible with the data [7, 8]. The present problem belongs to the second class: the specification gives a hard bound of one degree on every bearing, supplies no error statistics, and asks for a localisation region and its diameter rather than a confidence ellipse. Working with sets also removes the linearisation, which matters because the observation geometry can be nearly singular.

Three obstacles shape the analysis. First, the intersection of the angular domains can be unbounded, and in that regime a finite bounding box returns a finite but meaningless answer, so boundedness must be decided analytically. Second, the region is characterised as much by the smallest disk that contains it as by its diameter; the two measures coincide only in special cases, and whether the disk spanning the diameter covers the region is a covering question rather than a diameter question, with Jung's theorem [9] fixing the possible gap. Third, the second measurement is placed before the source position is known, so the design criterion must hold over every admissible source position and every admissible reading error, which leads to a minimax problem rather than to the maximisation of a nominal accuracy.

The paper makes three contributions. (i) It gives a set-membership localisation method whose output is the complete set of admissible positions, together with an analytic boundedness criterion that separates genuine degeneracy from the finite-box artefact. (ii) It separates the two error measures of that set, the diameter and the minimum enclosing circle (MEC), shows that the diameter disk does not always cover the region, and quantifies the gap by the two-sided Jung bound and a configuration that attains its upper end. (iii) It formulates the second detection point as a minimax-robust design over both the unknown source position and the unknown sign of the second bearing error, constrains it by worst-case reception, and reduces the search to the boundary of a robust feasible region. The next section states the problems, the two sections that follow develop the localisation geometry, the subsequent section develops the robust design, and the final section reports the experiments.

2. Problem Formulation

2.1. Measurement Model and Notation

A source G lies in a circular target region Ω of radius $R\Omega = 1800$ m centred at the origin; x points east, y points north, and azimuths are measured counter-clockwise from x. At each of n detection points $S_i = (x_i, y_i)$ a direction finder reports the bearing θ_i. Environmental conditions and instrument accuracy bias the reading, and the error magnitude does not exceed $\varepsilon = 1°$. Within one run the electromagnetic environment is fixed, so a repeated measurement at the same point carries no new information; only measurements at different positions are independent.

A bearing fixes the direction from S_i to G but not the distance. The positions compatible with a single reading form the angular domain

$$A_i = \{ P \in \mathbb{R}^2 : \angle(S_i \to P) \in [\theta_i - \varepsilon, \theta_i + \varepsilon] \}, \quad (1)$$

a cone of aperture 2ε with apex S_i, and the localisation region is its intersection with the target disk,

$$R = \Omega \cap A_1 \cap \cdots \cap A_n. \quad (2)$$

R is convex, because the angular domains and the disk are convex, and it contains the true source whenever the observations are consistent, so membership of the source in R is the strongest data-level check available. Two error measures are attached to it: the diameter $D = \max\{|P - Q| : P, Q \in R\}$, the largest distance between two admissible positions and the worst-

ISSN: 2688-8645

case localisation error used in the statement; and the radius R_{min} of the smallest disk containing R, the quantity a covering argument requires. They coincide only in special cases.

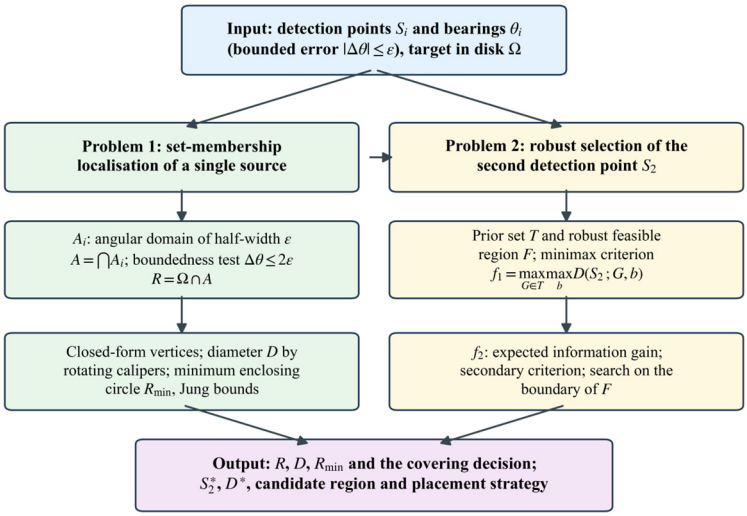


Figure 1. Structure of the set-membership localisation and detection-point selection procedure developed in this paper.

2.2. Statement of the Two Problems

Figure 1 summarises the solution chain. Problem 1 asks for a computable description of R, its diameter D, and a decision as to whether the disk whose diameter is the segment realising D covers R, together with the true MEC radius when it does not. Problem 2 assumes that a single detection point S_1 and its bearing θ_1 are known and asks for a selection strategy for a second point S_2, for the executable candidate region from which S_2 may be chosen, and for a recommended point, balancing observation geometry, reception reliability and travel cost.

2.3. Assumptions

Table 1. Main symbols.

Symbol	Meaning	Unit or value
S_i, θ_i	detection point index and bearing	m, (0°, 360°)
ε	bound on the bearing error	1°
A_i, A	angular domain of one observation and their intersection	—
Ω, R	target disk (radius 1800 m) and localisation region	m
D	diameter of R	m
R_{min}	radius of the minimum enclosing circle of R	m
δ, ρ	covering gap and covering ratio $R_{min}/(D/2)$	m, ≥ 1
T, F	prior set of the source and robust feasible region of S_2	—
f_1, f_2	worst case diameter and information gain	m, nat
β	angular offset of S_2 from the first bearing ray	°

Table 1 collects the notation used below. (1) The bearing error is bounded and directionally unbiased, $|\varphi_i - \theta_i| \le \varepsilon$, so the source lies in every angular domain. (2) Repeated bearings from one point carry no new information. (3) The problem is planar, the detection points are exact, and the height difference between finder and source is neglected. (4) A reported bearing implies that the source is within the effective reception radius, and one measurement corresponds to one source. (5) The source lies in the disk of radius 1800 m; when the angular intersection is unbounded it constrains only the direction, and the disk restores boundedness. (6) For Problem 2 the effective reception radius is not returned by the interface and lies in

ISSN: 2688-8645

[1000, 1500] m, so the design uses its worst value, 1000 m. (7) A valid bearing exists at S_1; because the optical probe resolves the source exactly within 20 m, and a second point is then unnecessary, the prior set keeps distances from 20 m to 1500 m. The point moves at 5 m/s, so a displacement of L metres costs L/5 seconds, and the source is stationary between the two measurements.

3. Set-Membership Localization under Bounded Bearing Errors

3.1. Angular Domains in Half-plane Form

Azimuths are first reduced to a common branch, $\theta \leftarrow \theta \bmod 2\pi$, and angular differences are evaluated as

$$\mathrm{wrap}(\Delta) = (\Delta + \pi) \bmod 2\pi - \pi \in (-\pi, \pi], \tag{3}$$

so that 359° and 1° are not mistaken for a difference of 358°. Each boundary ray of A_i is a line $a\,x + b\,y = c$, with coefficients fixed by its direction; the angular domain is therefore the intersection of two half-planes, and the localisation region is a convex polygon, This representation makes convexity, vertex enumeration, point-in-region tests and clipping standard operations, and it is reused at every step of the later search. The intersection $A = A_1 \cap \cdots \cap A_n$ may be unbounded even though R is always bounded by Ω; the boundedness test therefore applies to A and the truncation to Ω, and the two operations must not be interchanged. When the data are consistent, R is normally a quadrilateral for n = 2, but redundant constraints or a detection point inside another angular domain can reduce it to a triangle, a segment or a point.

$$R = \Omega \cap \{\, P : a_k\, x + b_k\, y \le c_k\,,\ k = 1, \ldots, 2n \,\}. \tag{4}$$

3.2. An Analytic Boundedness Criterion

Treat each observation as a closed interval $I_i = [\theta_i - \varepsilon, \theta_i + \varepsilon]$ on the circle. The intersection of the angular domains is unbounded exactly when the intervals share a direction:

$$A \text{ unbounded} \iff \exists\, r :\ \max_j \mathrm{wrap}(\theta_j - \theta_r) - \min_j \mathrm{wrap}(\theta_j - \theta_r) \le 2\varepsilon. \tag{5}$$

For n = 2 this reduces to $|\theta_1 - \theta_2| \le 2\varepsilon$, so the critical value is exactly 2°. The proof is one line: a set is unbounded if and only if its recession cone is non-empty, the recession cone of A_i is precisely I_i, and $\mathrm{rec}(A) = \cap_i I_i$ is non-empty exactly when some direction lies within ε of every observed bearing. When A is unbounded the bearings fix the direction but not the distance, and the shape of R is dictated by the disk. Just above the critical value A is bounded but degenerates into a thin blade of enormous diameter, so results obtained close to 2ε are unusable in practice and must be reported as such. For three or more intervals the pairwise form is weaker than the existence of a common direction, because intervals can intersect pairwise without sharing a point; in the parameter range of this paper the two forms coincide.

3.3. Truncation by the Target Disk

When A is unbounded or extends beyond the target region, R is truncated by the disk of radius 1800 m. The disk is replaced by a regular N-gon (N = 1440) on the same half-plane representation: the inscribed and circumscribed polygons bracket the true diameter, and at this N their difference is below 5×10^{-3} m, which is negligible relative to the diameters reported here.

ISSN: 2688-8645

4. Diameter and Minimum Enclosing Circle

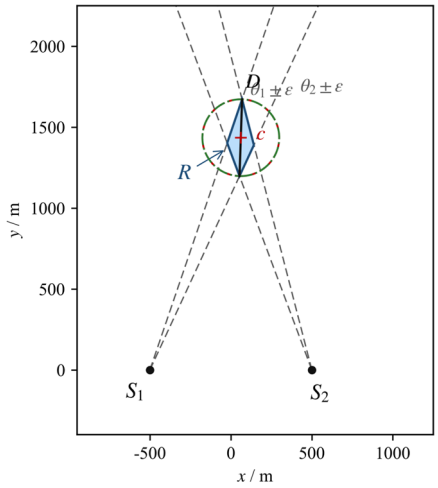


Figure 2. Two-station intersection: the localisation region R (shaded), the segment that realises its diameter D, the disk of radius D/2 (dashed) and the minimum enclosing circle (dash-dotted). The bearing error is exaggerated to ±3° for legibility.

4.1. Closed-form Vertices for Two Detection Points

For two detection points the vertices follow in closed form. Let O be the intersection of the two bearing centre lines, take O as origin and $S_1 \to O$ as the positive x axis, so that $S_1 = (-p, 0)$ and $S_2 = -q\,(\cos\gamma, \sin\gamma)$. The four candidates, indexed by $a, b \in \{-1, +1\}$, are

$$t_{ab} = [\, p \sin(\gamma + b\varepsilon) - q \sin(b\varepsilon) \,] \,/\, \sin(\, \gamma + (b - a)\varepsilon \,), \quad V_{ab} = S_1 + t_{ab}\,(\, \cos(a\varepsilon), \sin(a\varepsilon) \,), \tag{6}$$

and a candidate is admissible when it lies on the positive side of both rays,

$$s_{ab} = [\, q \sin(a\varepsilon - \gamma) - p \sin(a\varepsilon) \,] \,/\, \sin(\, a\varepsilon - \gamma - b\varepsilon \,), \quad t_{ab} > 0 \ \text{ and } \ s_{ab} > 0. \tag{7}$$

The region is the convex hull of the admissible candidates, obtained in constant time. One completion is needed: when the source is close to a detection point, that point falls inside the other angular domain and the region degenerates to a triangle with S_i as a vertex, which the four candidates miss; S_i is therefore added to the candidate set. Figure 2 shows a two-station region with its diameter, the disk of radius D/2 and the MEC.

4.2. Diameter and its Behaviour

Because R is a convex polygon, its diameter is attained at a pair of vertices:

$$D = \operatorname{diam}(R) = \max_{j<k} |V_j - V_k|. \tag{8}$$

The maximum of the convex function $|P - Q|$ over a convex set is attained at extreme points; for m vertices, comparing all pairs costs $O(m^2)$ and rotating calipers [10] costs O(m). The implementation uses calipers and checks the result against exhaustive enumeration. Two scalings are worth recording. For small ε the region contracts to a parallelogram whose half-diagonals point along the two bearings, so $D \propto \varepsilon / \sin\gamma$ and the accuracy degrades as the intersection angle γ shrinks. When the baseline and the bearing direction are nearly parallel, with the two bearings differing by Δθ, the diameter behaves as $D = d \sin\varepsilon / \sin(\Delta\theta - 2\varepsilon)$ and diverges as $\Delta\theta \to 2\varepsilon^{+}$; this is the quantitative form of the warning in the analytic boundedness criterion, and it shows that no finite accuracy can be quoted near the critical value.

4.3. Covering Test and Jung Bounds

The third part of Problem 1 asks whether the disk whose diameter is the segment realising D covers R. Let $c = (V_u + V_v)/2$ be the midpoint of a diameter segment. The covering gap is

$$\delta = \max_k |V_k - c| - D/2\,, \quad \text{with } \ \delta \le 0 \ \text{ if and only if the disk covers R.} \tag{9}$$

ISSN: 2688-8645

Both R and the disk are convex, so the disk covers R exactly when it covers the vertices. For a diameter pair (A, B) the vertex test reduces to the Thales condition

$$(P - A) \cdot (P - B) \le 0 \ \ \forall P \in V \ \ \Leftrightarrow \ \ \text{disk}(AB) \text{ covers } R \ \ \Leftrightarrow \ \ R_{\min} \le D/2. \tag{10}$$

The two measures are linked by Jung's theorem [9], which states that any planar set of diameter D lies in a disk of radius at most $D/\sqrt{3}$:

$$D/2 \le R_{\min} \le D/\sqrt{3}\,, \quad 0 \le \delta \le (\,1/\sqrt{3} - 1/2\,)\,D \approx 0.0774\,D. \tag{11}$$

The left inequality is an equality exactly for centrally symmetric regions, where the diameter disk already covers R; the right one is attained by the equilateral triangle, whose MEC has radius $D/\sqrt{3}$ (Figure 3). The ratio $\rho = R_{\min}/(D/2)$ therefore lies in $[1, 2/\sqrt{3}] = [1, 1.154700538]$. In practice the covering question must be answered either by constructing the true MEC or by verifying the Thales condition at every vertex; assuming that the diameter disk covers the region is not admissible.

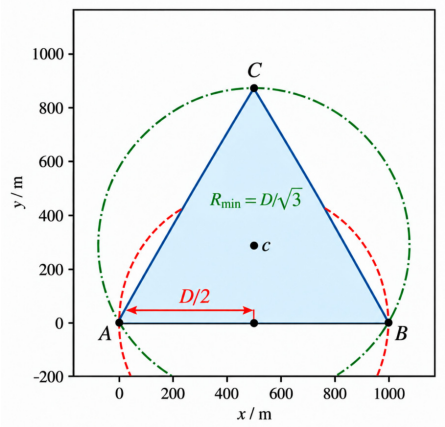


Figure 3. Equilateral-triangle counterexample. The disk having a side AB as its diameter, of radius D/2 (dashed), leaves the third vertex outside, while the minimum enclosing circle has radius $D/\sqrt{3}$ (dash-dotted). The ratio $\rho = 2/\sqrt{3}$ is the largest value admitted by Jung's bound (11).

4.4. Computing the Minimum Enclosing Circle

The MEC of a vertex set is determined by two or three of its points: if the boundary passed through one point only, moving the centre away from it would reduce the radius while still covering the set. It is therefore enough to test every two-point circle (centre at the midpoint, radius half the distance) and every three-point circumcircle, keep those that cover all vertices and take the smallest. For the few vertices of a two-station region this enumeration is negligible and exact; the implementation cross-checks it against Welzl's randomised incremental algorithm [11], and the two agree to 10^{-10} m. For regions truncated by the disk, the arc extreme points are added to the vertex set before the enumeration.

4.5. The Two Covering Cases

The gap δ depends on the shape of R, not merely on the number of observations. For a two-station intersection it is negligible: in the quadrilateral case δ vanishes identically, and in the degenerate triangular case it is positive but at most 4.86×10^{-3} of D/2 over the parameter grid examined. With three or more observations it can no longer be ignored: the proportion of configurations in which the diameter disk fails to cover R rises to 13–21 %, with a maximum ratio of 1.135536, still below the Jung bound. Figure 4 compares the two situations at a common scale. The practical conclusion is that the covering decision is case-by-case, and that in multi-observation problems the MEC, rather than the diameter disk, is the safe description.

ISSN: 2688-8645

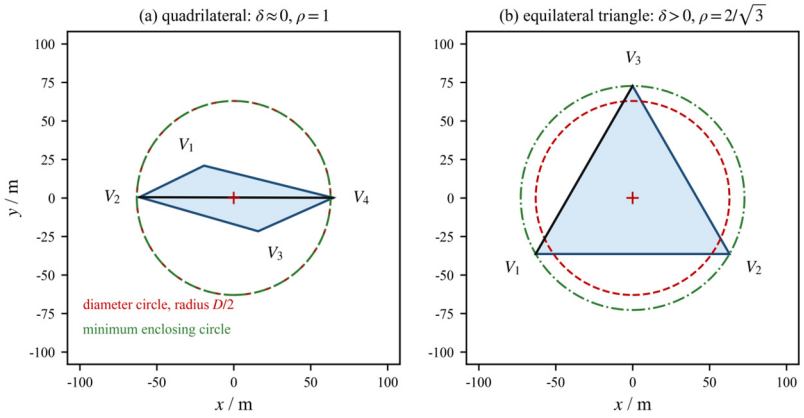


Figure 4. The two covering cases at a common scale. (a) A quadrilateral region, for which the diameter disk coincides with the minimum enclosing circle and $\delta \approx 0$. (b) An equilateral-triangle region, for which the diameter disk leaves the third vertex outside and $\rho = 2/\sqrt{3}$ attains the upper end of Jung's bound.

5. Robust Selection of the Second Detection Point

The second point is a sequential sensor-placement decision, a one-step instance of the next-best-view and coverage-planning problem [12]. It must be made before the source position is known, which is what turns the design into a minimax problem.

5.1. Prior Set and Robust Feasible Region

A single bearing gives a direction but no distance. Under assumptions (6) and (7) the positions compatible with the observation at S_1 form the intersection of an angular domain, an annulus and the target disk:

$$T = \{ P \in \mathbb{R}^2 : \angle(S_1 \to P) \in [\theta_1 - \varepsilon, \theta_1 + \varepsilon],\ 20 \le |P - S_1| \le 1500,\ |P| \le 1800 \}. \quad (12)$$

T is a narrow wedge of half-angle ε whose far end is cut by the disk. Its inner boundary reflects the fact that the optical probe resolves the source within 20 m, so no second point is needed there. The far end is the exit distance from the disk, where u is the unit vector of the bearing ray. T is not convex because the near end is hollowed out, but $|S_2 - G|$ is convex in G, so its maximum over T equals its maximum over the convex hull of T and is attained at one of the four wedge corners or on one of the two arcs.

$$d_{exit} = -(S_1 \cdot u) + \sqrt{((S_1 \cdot u)^2 - |S_1|^2 + 1800^2)}, \quad (13)$$

The second point must lie in the target region and must be able to receive the source even at the least favourable position of T and at the worst-case reception radius. The robust feasible region is therefore

$$F = \{ S_2 : |S_2| \le 1800,\ \max_{G \in T} |S_2 - G| \le R_{design} \}. \quad (14)$$

The inner maximum has a closed form. Writing ψ for the azimuth from S_1 to S_2, the farthest point of the wedge is

$$\varphi^* = \psi + 180^\circ \text{ if it lies inside the interval, otherwise at an arc endpoint,} \quad (15)$$

that is, the point facing away from S_2 or an arc endpoint, whichever is farther. A cross-check on 385 random candidates showed the analytic value to be never smaller than a dense sampling estimate, the largest discrepancy being 0.9 m caused by sampling missing an interior arc extreme point. Because the optimum sits on the boundary of F, this precision matters. Figure 5 shows T and F.

ISSN: 2688-8645

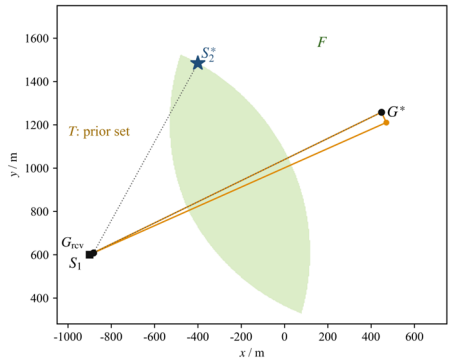


Figure 5. Prior set T and robust feasible region F. T is a narrow wedge of half-angle ε = 1° (its four discrete corners are marked); F is the reception-feasible region of (14), bounded by two arcs of radius R_{design}. The optimum S_2^* lies on the boundary of F, where the reception constraint is active at G_{rcv}, with $|S_2^* - G_{rcv}| = 1000$ m

5.2. Minimax Criterion: Worst-case Localisation Diameter

At S_2 each admissible source G produces a second bearing with error bounded by ε, so the localisation region is the intersection of the observed first angular domain with an ε-sector about that bearing. Two features make the design criterion a genuine worst case. First, θ_1 is already data: T is the exact posterior set given that reading, and no further worst-casing over its error is meaningful. Second, the second reading has not yet been taken; its error can have either sign, and the two signs produce regions of different size. The criterion therefore maximises over the source position and over the sign $b \in \{-1, +1\}$ of the second reading error:

$$f_1(S_2) = \max_{G \in T} \max_{b \in \{-1,+1\}} D(S_2; G, b). \quad (16)$$

For fixed S_2, G and b the two error sectors are bounded by four rays; their pairwise intersections, together with the two cone apices when admissible, give six candidates, and after filtering they form a polygon whose diameter is

$$D(S_2; G, b) = \max_{1 \le i < j \le 6} |V_i - V_j|. \quad (17)$$

Omitting b — that is, centring the second sector on the true bearing — understates the worst-case diameter by 4.3 % at the recommended point (125.90 m instead of 131.36 m), which is exactly the optimism a robust criterion must avoid. Figure 6 shows the worst-case region at the optimum, where the adverse sign places G* on the boundary of the second sector.

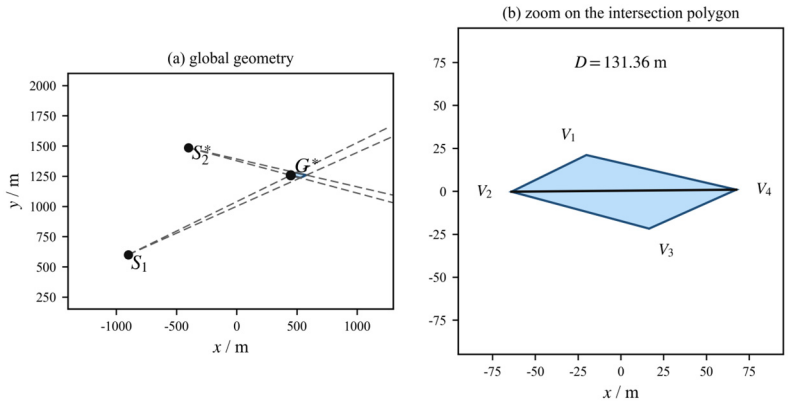


Figure 6. Construction of the worst-case localisation region. (a) Global geometry: the two pairs of error rays from S_1 and S_2^* around the worst admissible source G*. (b) Enlarged view of the intersection polygon; its diameter is $D(S_2^*; G^*, +\varepsilon) = 131.36$ m

ISSN: 2688-8645

5.3. Secondary Criterion and Decision Rule

Minimising the worst-case error alone can select a point that is geometrically sound yet uninformative, so a secondary criterion is used: the expected information gain about the source position, estimated by sample retention: admissible sources are drawn from T, an observation is generated for each, the fraction p that remains compatible is computed, and f_2 is the sample mean of −ln p. Over the feasible region f_1 and f_2 trade off along a Pareto front, but the trade-off is flat: the knee point raises the worst-case diameter by only 1.7 % and is therefore not adopted. The recommended design is the minimax point, with f_2 used only to choose between the two mirror solutions and to grade the candidate region.

$$f_2 (S_2) = H(T) − E[H(T \mid \text{observation})] = I(\text{source position} ; \text{bearing at } S_2), \quad (18)$$

Travel enters as a constraint rather than as a third objective. The recommended point is 1016 m from S_1, a travel time of 203.2 s at 5 m/s; because it lies on the reception boundary, no shorter move preserves the worst-case reception guarantee. If the time budget is below about 205 s, the same criterion restricted to a smaller radius is used, which trades accuracy for mobility without changing the method.

5.4. Recommended Point and Candidate Region

The reference setting is S_1 = (−900, 600) m, θ_1 = 25°, ε = 1°, R_{design} = 1000 m, target radius 1800 m and prior distance interval [20, 1500] m. The minimax optimum and two control criteria are listed in Table 2.

Table 2. Optimal second detection point under three criteria.

Criterion	S_2^* / m	Distance to S_1 / m	Objective value
worst case diameter (primary, this paper)	(−399.6586, 1484.2672)	1016.007	D* = 131.36 m
GDOP (worst case, control)	(−401.2023, 1485.1149)	1015.986	2650.4167
Bayesian VaR95(GDOP) (control)	(−336.5067, 1446.4259)	1016.839	2245.5843

Relative to S_1 the primary solution has local coordinates (a, b) = (827.1708, 589.9648) m in the frame rotated by θ_1, i.e. it is offset from the first bearing ray by β = 35.5°. The mirror solution b → −b is at (99.0012, 414.8878) m. Constraint checks give $|S_2^*|$ = 1537.1 m, so the disk constraint is inactive, while the reception constraint is active: $\max_{G \in T} |S_2^* − G|$ = 1000 m, attained at G_{rcv} = (−881.7, 608.1) m, the inner corner of T at d = 20 m and δ = −1°. The source hardest to receive and the source hardest to localise are different points: the worst-case diameter is attained at G* = (448.19, 1257.56) m, d = 1500 m and δ = +1°, whose distance to S_2^* is 877.6 m and which therefore does not touch the reception boundary.

Table 3. Grading of the candidate region on a 10 m grid.

Accuracy criterion	Grid points	Radius interval from S_1 / m
robust feasible region F	4653	—
D ≤ 1.05 D*	107	[987, 1016]
D ≤ 1.20 D*	482	[912, 1018]
D ≤ 250 m	1677	[728, 1019]

ISSN: 2688-8645

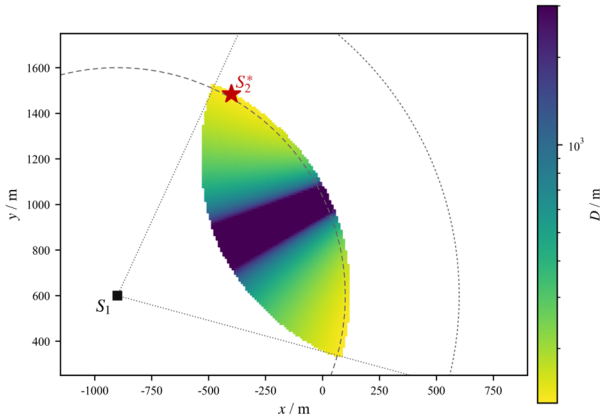


Figure 7. Grading of the candidate region for the second detection point. Each point of the 10 m grid inside the robust feasible region is coloured by the worst-case diameter it achieves (logarithmic colour scale, capped at 3000 m); the two dotted rays delimit the angular extent of about ±40.2°, and the recommended point S_2^* lies on the reception-constrained boundary.

The angular extent of the candidate region is fixed at ±40.2° by the reception constraint, while its radial width grows as the accuracy requirement is relaxed: the band within 5 % of D* is about 30 m wide in radius, and the band within 20 % is about 106 m wide. Table 3 and Figure 7 grade the feasible region. Three rules summarise the strategy. (i) Push S_2 to the robust reception boundary, so that the least favourable source is exactly at the worst-case reception radius; this neither wastes travel nor risks losing the signal. (ii) Offset S_2 from the first bearing by a fixed angle, 35.5° here with a practical range of 30°–40°, so that the intersection angle approaches 90°. (iii) Choose within the candidate region by accuracy grade, and when both mirror regions are available take the side closer to the current position.

6. Numerical Experiments and Sensitivity Analysis

6.1. Verification

The two models were checked by a single self-contained script that compares each conclusion with an independent implementation. Table 4 condenses the programme: the closed-form vertices are compared with a half-plane intersection, the boundedness test is scanned across its critical value, the covering tests and the two MEC algorithms are compared on random configurations, and the degeneracy and failure-to-cover rates are measured on large samples. The largest discrepancy between the vertex constructions is 3.21×10^{-10} m over 2000 configurations; the boundedness test switches between 2.000° and 2.001°; the three covering tests agree in all 1500 bounded configurations; the equilateral family reproduces $\rho = 2/\sqrt{3}$ to machine precision; and the failure-to-cover rate is 1.04 %, 12.76 % and 20.41 % for n = 2, 3 and 4.

Table 4. Condensed verification of the models of Problems 1 and 2.

Property	Test	Result
vertices, convexity, vertex count	2000 random cases against half plane intersection	no disagreement; max deviation 3.21×10^{-10} m
boundedness criterion	n = 2 scan, detection points 1000 m apart	$\Delta\theta \le 2.000°$ unbounded; 2.001° bounded, D = 9.99×10^5 m
diameter, covering tests, MEC	1500 cases; three covering tests; two MEC algorithms	all agree; $D/2 \le R_{min} \le D/\sqrt{3}$; ratio exactly $2/\sqrt{3}$
covering gap, many observations	14885 grid cases; n = 2, 3, 4 samples	max $\delta/(D/2) = 4.86 \times 10^{-3}$; failure to cover 1.04 %, 12.76 %, 20.41 %

ISSN: 2688-8645

6.2. Comparison with a Naive Placement

To quantify the benefit of the robust design, the worst-case diameter was evaluated on 3000 sources drawn uniformly from T. At the recommended point the mean diameter is 56.3 m, the median 49.6 m and the 90th percentile 93.6 m. A layout that places S2 at 1000 m from S1 perpendicular to the first bearing, ignoring the prior set and the reception constraint, gives 95.0 m, 81.2 m and 178.1 m. The improvement is therefore concentrated in the tail, which is the part that matters when the diameter is used as a worst-case bound. For reference, the Pareto knee gives a mean of 57.8 m, within 3 % of the optimum.

6.3. Sensitivity and Limitations

Three sensitivities were examined. The inner bound d_{lo} = 20 m changes the optimum by only 1.9 %, so the exact optical-probe range is not critical. Replacing R_{design} = 1000 m by the nominal 1500 m does not change the active constraint, because the binding source is the inner corner of T; the boundary of F moves but the optimum stays on it. A full 10 m grid enumeration gives an objective 0.16 % worse, which corroborates the optimum rather than proving global optimality.

Two limitations remain. The outer search is a local refinement, and the inner worst value is obtained numerically, so no global optimality proof is claimed. The closed-form vertices are specific to two detection points; for three or more observations the region is still a convex polygon and the diameter and MEC algorithms apply unchanged, but the vertices must be obtained by half-plane intersection, and the covering gap becomes markedly larger, so the MEC rather than the diameter disk should be used.

7. Conclusion

This paper has developed a set-membership treatment of the first two stages of interference-source localisation under a bounded bearing error. Bearings are represented as angular domains, and the set of admissible positions is their intersection with the target disk. Three results are central. First, boundedness of the angular intersection is decided analytically by (5), which for two observations reduces to $\Delta\theta \le 2\varepsilon$ and resolves the near-degenerate regime in which a finite bounding box returns a finite but meaningless answer. Second, the diameter of R and the radius of its MEC are distinct error measures: the diameter disk does not always cover R, the two are linked by $D/2 \le R_{min} \le D/\sqrt{3}$, and the upper end is attained by an equilateral configuration. The covering question is settled either by the true MEC or by the Thales test at every vertex.

Third, the second detection point is a minimax problem over both the unknown source position and the unknown sign of the second reading error. Taking the worst-case diameter as the criterion, the optimum lies on the boundary of the robust feasible region, offset from the first bearing by 35.5°, with a worst-case diameter of 131.36 m; its mirror is equivalent, and the candidate region is an annular sector of half-width 40.2°. A Monte-Carlo study shows that the gain over a naive perpendicular placement is concentrated in the tail of the error distribution, as a worst-case criterion should be. Two extensions are natural: replacing the two-station closed form by half-plane intersection for three or more observations, and embedding the geometry in the multi-source scheduling problem, where the same region and diameter serve as the localisation primitive.

References

[1] Langley, R. B. (1999). Dilution of precision. GPS World, 10(5), 52–59.

[2] Nardone, S. C., Lindgren, A. G., & Gong, K. F. (1984). Fundamental properties and performance of conventional bearings-only target motion analysis. IEEE Transactions on Automatic Control, 29(9), 775–787. https://doi.org/10.1109/TAC.1984.1103671.

[3] Torrieri, D. J. (1984). Statistical theory of passive location systems. IEEE Transactions on Aerospace and Electronic Systems, 20(2), 183–198. https://doi.org/10.1109/TAES.1984.310435.

[4] Dogancay, K. (2005). Bearings-only target localization using total least squares. Signal Processing, 85(9), 1695–1710. https://doi.org/10.1016/j.sigpro.2005.01.012.

[5] Bishop, A. N., Fidan, B., Anderson, B. D. O., Dogancay, K., & Pathirana, P. N. (2010). Optimality analysis of sensor-target localization geometries. Automatica, 46(3), 479–492. https://doi.org/10.1016/j.automatica.2009.12.003.

[6] Jiang, H., Cai, Y., & Yu, Z. (2022). Observability metrics for single-target tracking with bearings-only measurements. IEEE Transactions on Systems, Man, and Cybernetics: Systems, 52(2), 1065–1077. https://doi.org/10.1109/TSMC.2020.3044040.

[7] Jaulin, L., Kieffer, M., Didrit, O., & Walter, É. (2001). Applied interval analysis. Springer.

[8] Zhu, Y., Fang, X., & Li, C. (2025). Multi-sensor information fusion for mobile robot indoor-outdoor localization: A zonotopic set-membership estimation approach. Electronics, 14(5), 867. https://doi.org/10.3390/electronics14050867.

[9] Jung, H. (1901). Über die kleinste Kugel, die eine räumliche Figur einschließt. Journal für die reine und angewandte Mathematik, 123, 241–257.

[10] Toussaint, G. T. (1983). Solving geometric problems with the rotating calipers. In Proceedings of the IEEE MELECON (pp. A10.02/1–4). Athens, Greece.

[11] Welzl, E. (1991). Smallest enclosing disks (balls and ellipsoids). In H. Maurer (Ed.), New results and new trends in computer science (pp. 359–370). Springer. https://doi.org/10.1007/BFb0038194..

[12] Tan, C. S., Mohd-Mokhtar, R., & Arshad, M. R. (2021). A comprehensive review of coverage path planning in robotics using classical and heuristic algorithms. IEEE Access, 9, 119310–119342. https://doi.org/10.1109/ACCESS.2021.3107568.